Shear-Thickening Dilute Surfactant Solutions: Equilibrium Structure As Studied by Small-Angle Neutron Scattering

R. Gamez-Corrales and J.-F. Berret*

Unité Mixte de Recherche CNRS/Université de Montpellier II No. 5581, Groupe de Dynamique des Phases Condensées, F-34095 Montpellier Cedex 05, France

L. M. Walker

Department of Chemical Engineering Carnegie Mellon University, Pittsburgh, Pennsylvania 15213

J. Oberdisse

Laboratoire Léon-Brillouin, CEA Saclay, F-91191 Gif/Yvette, France

Received February 22, 1999. In Final Form: May 26, 1999

We have combined rheology and small-angle neutron scattering experiments to investigate dilute aqueous solution of cetyltrimethylammonium tosylate (CTAT). Rheology experiments have been performed under controlled strain conditions as function of concentration ($\phi = 0.05 - 1\%$) and temperature ($T = 23-45$ °C). At low surfactant concentration and under steady shear conditions, the CTAT exhibits a continuous increase of the apparent viscosity with increasing shear rates, also termed a shear-thickening transition. The critical shear rate for shear thickening varies strongly with the temperature according to an Arrhenius behavior, but very weakly with concentration. On the same solutions that were studied by rheology, neutron scattering was performed at rest to search for a correlation between the rheological features of the shear-thickening transition and the equilibrium micellar structure. We have found that (i) for all concentrations that display the thickening transition, the local morphology is that of cylindrical micelles, with a radius $R = 21.0 \pm 0.5$ Å; (ii) all spectra exhibit a scattering correlation peak due to strong electrostatic repulsion between charged micelles; (iii) the shear-thickening transition in CTAT displays the same rheological features for solutions prepared either in the dilute ($\phi < \phi^*$) or in the semidilute ($\phi^* < \phi < 0.8\%$) regimes.

I. Introduction

When exposed to a flow field, many dilute surfactant solutions exhibit drastic changes in their rheological properties. The rheological transition can be observed by simply shaking a jar of the sample. The solution will transform temporarily from a low-viscosity liquid into a viscoelastic liquid, as evidenced by the recoil of bubbles in the sample. Under controlled (simple) shearing conditions, this transition is characterized by an increase of the apparent viscosity of the fluid above a critical shear rate $\dot{\gamma}$ and is called a shear-thickening transition. Although our knowledge of the phenomenology of this shear-thickening transition has been improved noticeably,[1−7] the microscopic mechanisms and the nature of the transition remain an open debate. Even the specific colloidal properties necessary for the transition have not been identified.

Recently, there has been a renewed interest in the shear-thickening transition. New surfactants which exhibit the thickening behavior have been discovered, e.g., the Gemini surfactants,[8−10] and new techniques have been applied, such as transient flow birefringence,[7,8] light scattering microscopy,[11,12] electrical conductivity,[8] neutron scattering under shear,[13−15] and cryo-TEM of the shear-induced state.[8,10,16] The overall picture that emerges from this huge amount of experimental work is that of a shear-induced transition. Often described as a shear-induced structure (SIS)[5] or shear-induced phase (SIP),[12] this second state is not fully understood. The quantitative features of the shear-thickening transition are varying from one system to the other. However, all systems share in common some elementary characteristics: (i) shear thickening occurs for surfactants that self-assemble into cylindrical micelles;

* To whom correspondence should be addressed. E-mail: berret@gdpc.univ-montp2.fr.

(1) Hoffmann, H.; Platz, G.; Rehage, H.; Schorr, W.; Ulbricht, W. *Ber. Bunsen-Ges. Phys. Chem.* **1981**, *85*, 255−266.
(2) Rehage, H.; Hoffmann, H. *Rheol. Acta* **1982**, *21*, 561−563.
(3) Bewersdorff, H.-W.; Frings, B.; Lindner, P.; Oberthür, R. C. *Rheol. Acta* **1986**, 25.
(4) Lindner, P.; Bewersdorff, H.-W.; Heen, R.; Sittart, P.; Thiel, H.; Langowski, J.; Oberthür, R. C. *Prog. Colloid Polym. Sci.* **1990**, *81*, 107−112.
(5) Hoffmann, S.; Rauscher, A.; Hoffmann, H. *Ber. Bunsen-Ges. Phys. Chem.* **1991**, 95, 153−164.
(6) Wunderlich, A. M.; Brunn, P. O. *Colloid Polym. Sci.* **1989**, *267*, 627−636.
(7) Wunderlich, I.; Hoffmann, H.; Rehage, H. *Rheol. Acta* **1987**, *26*, 532−542.
(8) Oda, R.; Panizza, P.; Schmutz, M.; Lequeux, F. *Langmuir* **1997**, *13*, 6407−6412.
(9) Oda, R.; Panizza, P.; Schmutz, M.; Lequeux, F. *Cahier Rhéol.* **1997**, 101−106.
(10) Lu, B.; Li, X.; Scriven, L. E.; Davis, H. T.; Talmon, Y.; Zakin, J. L. *Langmuir* **1998**, *14*, 8−16.
(11) Liu, C. H.; Pine, D. J. *Phys. Rev. Lett.* **1996**, *77*, 2121−2124.
(12) Boltenhagen, P.; Hu, Y.; Matthys, E. F.; Pine, D. J. *Phys. Rev. Lett.* **1997**, *79*, 2359−2362.
(13) Hoffmann, H.; Hofmann, S.; Rauscher, A.; Kalus, J. *Prog. Colloid Polym. Sci.* **1991**, *84*, 24−35.
(14) Schmitt, V.; Schosseler, S.; Lequeux, F. *Europhys. Lett.* **1995**, *30*, 31−36.
(15) Berret, J.-F.; Gamez-Corrales, R.; Oberdisse, J.; Walker, L. M.; Lindner, P. *Europhys. Lett.* **1998**, *41*, 677−682.
(16) Keller, S. L.; Boltenhagen, P.; Pine, D. J.; Zasadzinski, J. A. *Phys. Rev. Lett.* **1998**, *80*, 2725−2728.

10.1021/la990187b CCC: $15.00
Published on Web 08/07/1999

(ii) when sheared at shear rates higher than $\dot{\gamma}_c$, an induction time or deformation is always necessary to induce the viscous state; (iii) in the shear-induced state, the solutions are birefringent, or equivalently show some neutron anisotropic scattering patterns; (iv) large positive normal stresses are observed in the steady state of shearing above $\dot{\gamma}_c$.

In this paper, we focus on the equilibrium micellar structure of shear-thickening surfactant solutions. Two questions drive this research: What are the necessary conditions for the observation of the shear-thickening transition in terms of concentration, local microstructure, and intermicellar interactions? What is the correlation between the rheological features of the shear-thickening transition and the equilibrium micellar structure? Here, we report on the binary surfactant system cetyltrimethylammonium tosylate/water (CTAT) that exhibits such a shear-thickening transition.[15] The binary system was chosen so that there is no influence of excess ionic species in solution. Rheology experiments have been performed under controlled strain conditions as a function of concentration ($\phi = 0.05-1.0$ wt %) and temperature ($T = 23-45$ °C). On the same solutions, we performed systematic small-angle neutron scattering experiments at equilibrium (no shear) to identify the different concentration regimes as well as the microstructure of the self-assembling micelles. In a previous report on CTAT,[15] the flow-structure relationship was addressed with the emphasis on the SANS data under shear. We provide here the complete set of small-angle neutron scattering (SANS) measurements on that system at rest.

II. Experimental Details

The cetyltrimethylammonium tosylate (CTAT) was purchased from SIGMA products (purity 99%) and used without further purification. Purity of the surfactant was verified using DuNoy ring tensiometry. The surface tension showed no minimum prior to the critical micellar concentration (cmc = 0.011 wt %), indicating that no surface active impurities are present in the CTAT.[17] For rheological measurements, the samples were prepared with protonated water that was purified by passing a Millipore water system. For the SANS work, deuterated water (D_2O) was preferred for contrast reasons. For both the mechanical and structural measurements, the CTAT concentrations ranged between 0.08 and 6%. We also investigated the shear-thickening transition as function of temperature, from 22.5 (which is the Krafft temperature for CTAT) to 40 °C. All rheological measurements were made using a Rheometrics fluid spectrometer (RFS II) equipped with a Couette configuration with controlled shear rate (outer diameter 34 mm, gap 1 mm; the outer geometry rotates). Temperature was controlled with a fluid bath that circulates fluid around the outer fixture. Mechanical measurements are reported as apparent viscosity, which is simply the ratio of measured shear stress and applied shear rate. As it is possible that the shear-induced fluid is no longer homogeneous in the gap of the rheometer, we report apparent viscosity for all shear rates. Small-angle neutron scattering experiments were carried out at ambient temperature on the PACE beamline of the Laboratoire Léon Brillouin (Saclay, France). Data were collected at two sample-to-detector distances 2 and 4.7 m with incident wavelengths $\lambda = 6$ and 10 Å, respectively, covering a wave vector range from 5×10^{-3} to 0.16 Å^{-1}. The incoherent background arising from the hydrogen atoms of the aliphatic chains was calculated using test solutions containing a mixture of H_2O and D_2O.

III. Results

III.1. Rheology. Figure 1 displays the general behavior of the shear-thickening transition observed in the CTAT system. Here, the steady shear stress $\sigma(\dot{\gamma})$ and the steady apparent shear viscosity $\eta(\dot{\gamma})$ are shown as function of the applied shear rate $\dot{\gamma}$ for a CTAT/H_2O solution at $\phi = 0.41\%$ (T = 23 °C). For this solution the shear-thickening transition occurs at the critical shear rate $\dot{\gamma} = 14 \pm 2$ s^{-1}. In the steady flow curve, three regimes can be distinguished. At low shear rates (regime I, $\dot{\gamma} < \dot{\gamma}_c$), the stress increases linearly with the rate with a slope $\eta_0 = 1.3 \pm 0.1$ mPa s; in other words, the fluid exhibits Newtonian behavior. At $\dot{\gamma}_c$, the viscosity increases with increasing shear rate, and deviates progressively from the Newtonian behavior. The transition from the pure Newtonian behavior to the shear-thickened state is continuous. The apparent viscosity in regime II passes through a maximum, at 16 times the value of the Newtonian regime η_0, and then shear thinning is observed (regime III). The flow behavior of Figure 1 has been observed for concentrations of CTAT $\phi < 0.8\%$ in both H_2O and D_2O and at temperatures between 22.5 (the Krafft temperature) and 40 °C. The value of the critical shear rate and magnitude of the maximum in viscosity vary with both concentration and temperature.

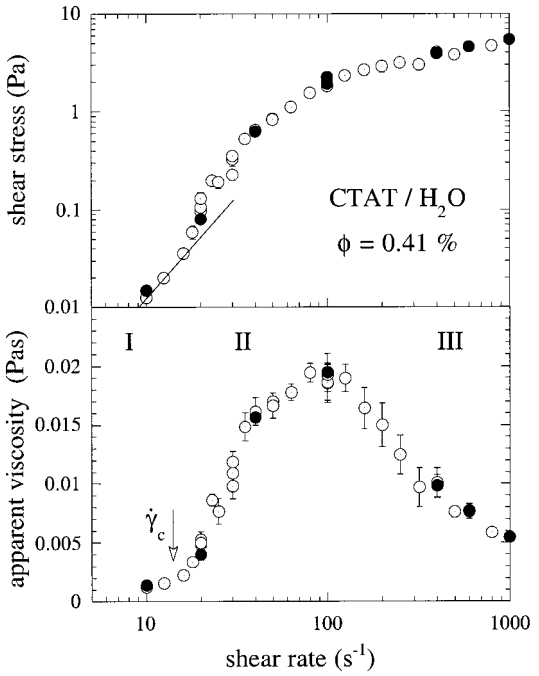

Figure 1. Steady-state shear stress (top) and viscosity (bottom) versus shear rate for 0.41% CTAT/H_2O at 23 °C. The shear-thickening transition occurs at $\dot{\gamma}_c = 14 \pm 2$ s^{-1} indicated by the arrow. Three regimes can be distinguished. At low shear rates (regime I, $\dot{\gamma} < \dot{\gamma}_c$), the fluid is Newtonian with a viscosity $\eta_0 =$ 1.3 mPa s. Above $\dot{\gamma}_c$ the viscosity increases continuously (regime II) and passes through a maximum, and then shear-thinning is observed (regime III).

Before discussing the temperature and concentration dependence of the steady flow curve, it is important to note that considerable care was taken to ensure that steady values of the stress were measured. All data points shown in Figure 1 are the result of transient mechanical measurements. Two specific procedures were utilized. The first procedure involved stepping down in applied shear rate from a steady preshear in regime III and then tracking the transients until a steady value of shear stress was achieved. This procedure yields the empty circles of Figure 1. The closed circles on this figure refer to steady-state values of the stress from solutions that were left free to equilibrate before shearing (i.e., no preshear). The two procedures result in the same values of steady apparent

(17) Thebaud, B. Carnegie Mellon University, 1998.

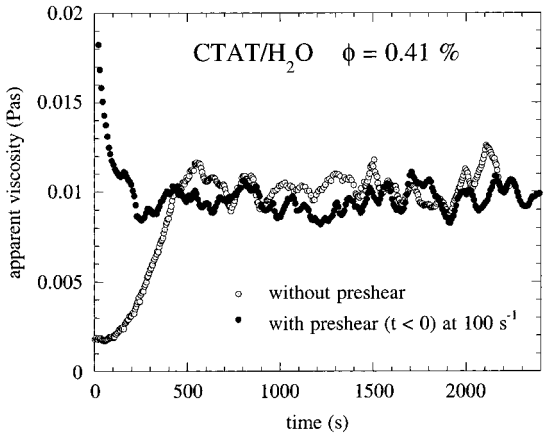

Figure 2. Transient responses of CTAT/H_2O ($\phi = 0.41\%$, $T = 23$ °C) subjected to a steady shear at $\dot{\gamma} = 30\ s^{-1}$ ($> \dot{\gamma}_c$). The closed circles refer to an experiment where the solution was left free to equilibrate before starting the measurement. The open circles correspond to an experiment where the solution was first presheared at a velocity gradient $\dot{\gamma}_{presh}$ higher than the critical one, $\dot{\gamma}_{presh} \gg \dot{\gamma}_c$. Both procedures yield the same values for the mechanical stresses and viscosities. The amplitudes of the oscillations in the transient viscosities are reproduced as error bars in Figure 1 (bottom).

viscosity; however, the duration of the transients was very different. An illustration of these transients is shown in Figure 2, for the same experimental conditions as in Figure 1 ($\phi = 0.41\%$, $T = 23$ °C, and $\dot{\gamma} = 30\ s^{-1}$). The first procedure with a preshear in regime III (at $100\ s^{-1}$) shows a decrease of the transient viscosity within the first 200 s, and then a stabilization around 9.8 ± 1.4 mPa s. In the second experiment, the stationary state is reached after an induction time of 600 s, but the stress or viscosity levels are the same. As for many dilute surfactant systems displaying shear-thickening transitions (e.g., ref 1), the stress in the steady state exhibits a noisy signal around a well-defined average. The amplitudes of the oscillations in the transient viscosities are reproduced as error bars in Figure 1 (bottom). We have not discussed so far the variation of the induction time as function of various parameters. Qualitatively the induction time becomes larger as shear rates approach $\dot{\gamma}_c$, but contrary to previous reports[18] we cannot report on any consistent dependence. Actually, the induction time was found to depend on the rheological history of the solution. This remarkable phenomenon will be investigated in detail in another study.

Figure 3a−c demonstrates both the temperature and concentration dependencies of CTAT rheology. The apparent shear viscosity as function of the shear rate for CTAT/D_2O at three concentrations, $\phi = 0.09$, 0.16, and 0.26%, in the temperature range $T = 25-36$ °C is shown in these figures. With increasing temperature, $\dot{\gamma}_c$ is shifted to higher rates by as much as two decades and the viscosity maximum in regime II lowers progressively. On the basis of these results, we find that above ~40 °C CTAT/D_2O does not display any thickening transition. To characterize the huge temperature dependence of the onset of shear thickening, we have plotted the critical rate $\dot{\gamma}_c$ versus the inverse absolute temperature at different concentrations. In these Arrhenius plots (Figure 4), straight lines are obtained that refer to a concentration-independent activation energy E_a. One finds for $\phi = 0.09$, 0.16, 0.26, and 0.41% in CTAT/D_2O an activation energy $E_a = (123 \pm 3)\ k_BT$, which corresponds to 306 kJ/mol.

(18) Boltenhagen, P.; Hu, Y.; Matthys, E. F.; Pine, D. J. *Europhys. Lett.* **1997**, *38*, 389−394.

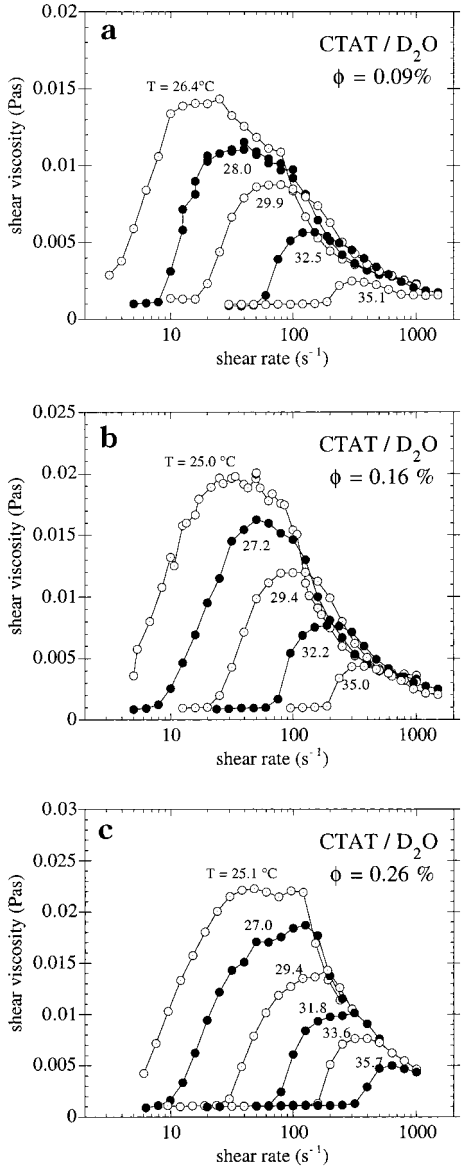

Figure 3. Temperature dependencies of the shear-thickening transition in CTAT/D_2O surfactant systems, for $\phi = 0.09$ (a), 0.16 (b), and 0.26% (c). As in Figure 1, all data points are taken under steady-state flow conditions. The deviation of the apparent viscosity from that of the solvent defines the critical shear rate $\dot{\gamma}_c$.

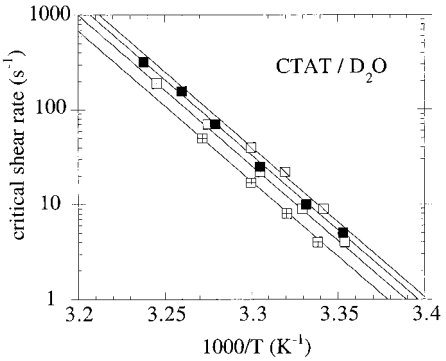

Figure 4. Arrhenius plot of the critical shear rates $\dot{\gamma}_c$ for CTAT/D_2O solutions at $\phi = 0.09$, 0.16, 0.26, and 0.41%. All four straight lines are with an activation energy $E_a = (123 \pm 3)\ k_BT$.

The concentration dependence of the rheological behavior is complex. It is interesting to look at the viscosity in regime I as a function of concentration. Figure 5 shows

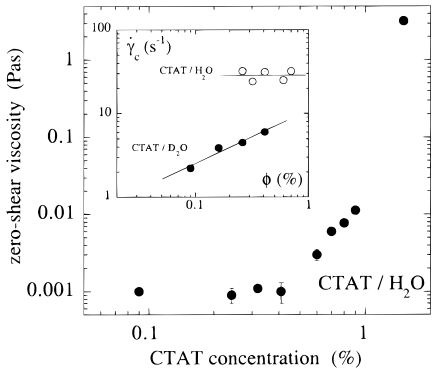

Figure 5. Variation of the static viscosity (in regime I) for CTAT/H_2O solutions at $T = 25$ °C as function of the concentration. Inset: Dependence of the critical shear rate $\dot{\gamma}_c$ on the surfactant concentration ϕ.

Table 1. Parameters Extracted from Rheology and SANS Data on CTAT/H_2O and CTAT/D_2O Surfactant Solutions

	ST-lower limit (%)	ϕ^* (%)	ST-upper limit (%)	E_a (in k_BT units)	α
CTAT/H_2O	∼0.05	$0.5^{(\eta)}$	∼0.9	116 ± 4	0 ± 0.05
CTAT/D_2O	∼0.05	$0.35^{(SANS)}$	∼0.8	123 ± 3	0.55 ± 0.05

[a] The so-called ST-lower and ST-upper (ST is used for shear thickening) limits denote the concentration boundaries in which the shear-thickening transition is observed. ϕ^* is the overlap concentration, E_a and α are the activation energies and power-law exponent featured in eq 1. The indexes (η) and (SANS) refer to results obtained using rheological experiments (Figure 5) and neutron spectroscopy (Figure 10), respectively.

the concentration variation of the static viscosity (in regime I) for CTAT/H_2O solutions at $T = 25$ °C. The viscosity is that of the solvent at low surfactant concentrations, and then increases tremendously as the solutions become viscoelastic. For surfactants forming elongated cylindrical micelles, these behaviors are not unusual. They are interpreted in terms of the transition between the dilute and the semidilute regimes of concentration,[19] similar to that seen in flexible polymer solutions.[20] The transition concentration is denoted ϕ^* in the following, and from rheology one gets $\phi^* \sim 0.5\%$ for CTAT/H_2O ($T = 25$ °C). One fundamental feature of the transition in CTAT is that the shear-thickening transition as described in Figure 1 occurs at concentrations well below (by a decade) and well above ϕ^*. Systems with 10 times the solvent viscosity cease to exhibit the shear thickening.[5] The concentration boundaries, as well as the overlap ϕ^* estimated for CTAT in water and in heavy water are summarized in Table 1. In the inset of Figure 5 are shown the dependencies of the critical shear rate $\dot{\gamma}_c$ as a function of the surfactant concentration ϕ. For CTAT/D_2O, $\dot{\gamma}_c(\phi)$ increases as a power law, with an exponent $\alpha = 0.55 \pm 0.05$. When the solvent is changed from D_2O to H_2O, $\dot{\gamma}_c(\phi)$ remains constant around 30 s^{-1}. The temperature and concentration dependencies can be summarized and expressed as

$$\dot{\gamma}_c(\phi,T) \sim \phi^{\alpha} \exp\left(-\frac{E_a}{k_BT}\right) \qquad (1)$$

The above findings seem to be fairly universal features of the shear-thickening transition. At least one of the two variations stated by eq 1,[5,6,8,9,2121] if not both, was already reported by different authors on other surfactant systems.

III.2. Small-Angle Neutron Scattering (SANS). SANS experiments were performed on the same CTAT solutions discussed above. Our goal was to determine the colloidal requirements for a solution to exhibit shear thickening. Figure 6 shows the absolute scattered neutron intensities from a series of CTAT/D_2O solutions ranging from 0.10 to 1.02% at 25 °C. All of the spectra exhibit a scattering maximum, at a wave vector denoted $q_{Max}(\phi)$ from this point on, which varies from 0.01 to 0.02 Å^{-1}. The location of this peak clearly depends on concentration. With increasing ϕ, the peak narrows progressively and, above ∼0.6%, a shoulder appears to the right of the peak. The continuous lines through the data points will be explained in section IV.3.

IV. Analysis of the Neutron Spectra

Here we analyze the neutron spectra to determine the colloidal properties of the surfactant aggregates at rest. We adopt two points of view, one semiquantitative based on the analysis of the asymptotic behaviors of the scattering intensity, and the second more quantitative founded on the derivation and fits of the scattered intensity in terms of form and structure factors of the aggregates.

IV.1. Local Microstructure: Radius and Persistence Length. The morphology of the aggregates is determined from the high q range of the neutron scattering. The first remarkable property exhibited by CTAT dilute solutions is illustrated in Figure 7. Here we have plotted on semilogarithmic scales the normalized intensity $I(q,\phi)/\phi$ versus q for ϕ ranging from 0.10 to 1.02%. Over one decade in concentration, all intensities at large wave vectors ($q > 0.05$ Å^{-1}) collapse onto the same master curve. The strong deviations observed at low q will be discussed later. We take the collapse of the high q intensity to be evidence that the microstructure being considered is identical at all ϕ. The next figure demonstrates that the local morphology is that of cylindrical micelles (Figure 8). Two spectra are shown at the concentration $\phi = 0.41\%$ and $T = 25$ °C. One solution is free of added salt (the data are those of Figure 6d) whereas the second was prepared with excess of sodium chloride (0.2 M NaCl). Again, in the high q range, both sets of data superimpose. However, in the low q region, the correlation peak observed for the salt-free solution is now suppressed and the intensity further increases. These two neutron intensities are now compared to the scattering resulting from an assembly of disordered cylindrical micelles of length L (monodisperse), as given by[22]

$$I(q) \approx 4\phi\Delta\rho^2\pi^2R^2\,\frac{1}{q}\left(\frac{J_1(qR)}{qR}\right)^2 \qquad (2)$$

where J_1 denotes the first-order Bessel function and $\Delta\rho = \rho_{D_2O} - \rho_{CTAT}$ is the difference in scattering length densities between the solvent and the surfactant. This equation is only valid if the total length of the micelles L is much larger than its radius R, so $L \gg R$ and the wave vector range is such that $qL \gg 1$. In these regimes, the variable L enters the scattering function through the volume fraction ϕ, which is known a priori (assuming a density of 1). At low q, such that $qR \ll 1$, eq 2 is dominated by the well-known $1/q$ dependence characteristic for cylindrical aggregates. For $qR \sim 1$ and above, the

(19) Oda, R.; Narayanan, J.; Hassan, P. A.; Manohar, C.; Salkar, R. A.; Kern, F.;Candau, S. J. *Langmuir* **1998**, *14*, 4364−4372.
(20) Ferry, J. D. *Viscoelastic properties of polymers,* 3rd ed.; John Wiley and Sons: New York, 1980.
(21) Hartmann, V.; Cressely, R. *J. Phys. II Fr.* **1997**, *7*, 1087−1098.
(22) Herbst, L.; Kalus, J.; Schmelzer, U. *J. Phys. Chem.* **1993**, *97*, 7774−7778.

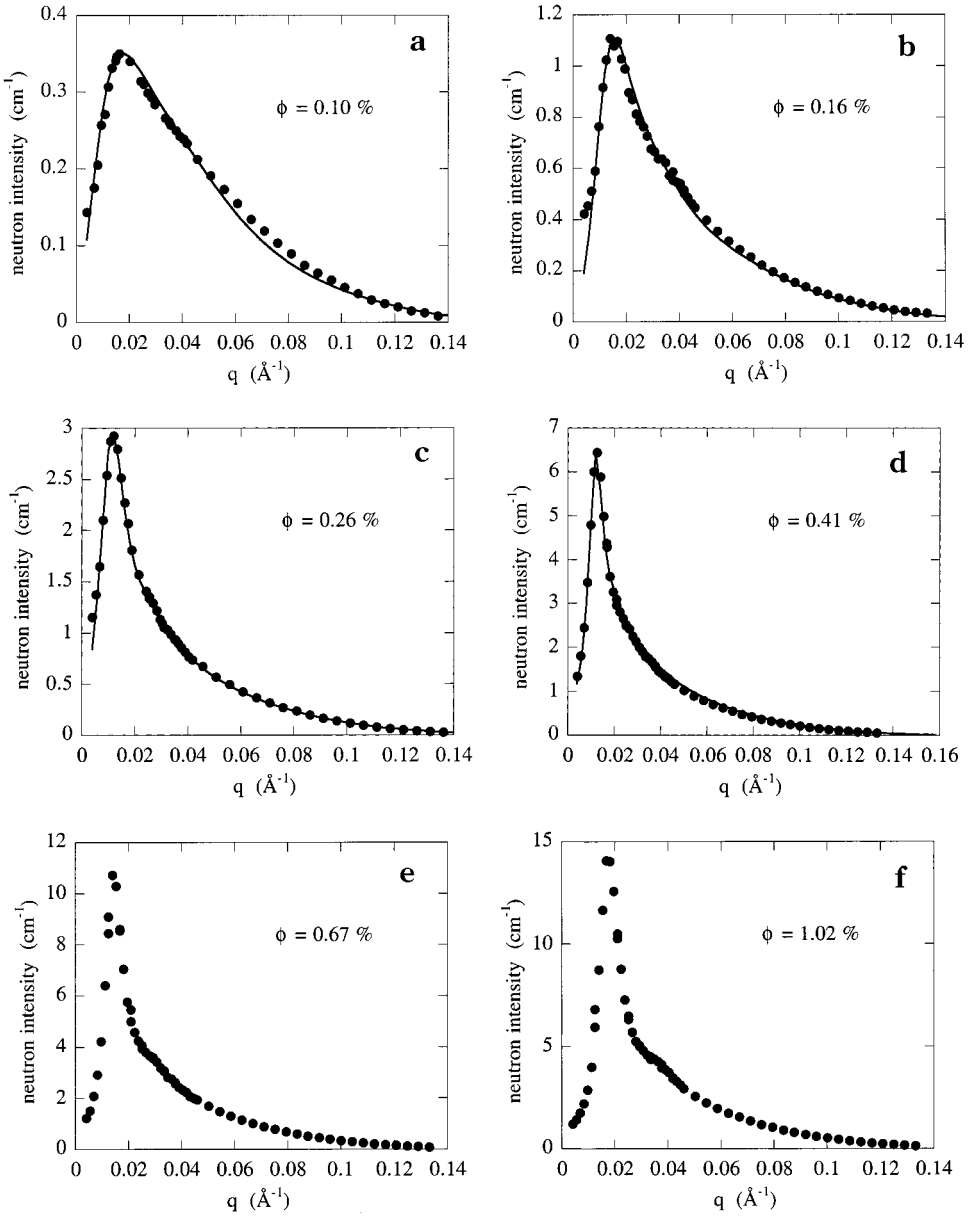

Figure 6. Absolute neutron intensities scattered by CTAT/D_2O solutions at $T = 25$ °C for concentrations $\phi = 0.10$ (a), 0.16 (b), 0.26 (c), 0.41 (d), 0.67 (e), and 1.02% (ϕ). All spectra exhibit a scattering maximum at the wave vector denoted $q_{Max}(\phi)$. The continuous lines through the data points result from best fit calculations using eqs 5 and 6, with parameters listed in Table 2.

scattering goes to 0 as the first oscillation of the form factor is approached ($qR = 3.8$). The high q data on CTAT are successfully compared to eq 2 with only two adjustable parameters, the radius $R = 21 \pm 0.4$ Å and the contrast $\Delta\rho = 6.12 \times 10^{10}$ cm^{-2}. A direct calculation for the scattering length density from CTAT provides $\rho_{CTAT} = 0.258 \times 10^{10}$ cm^{-2}, i.e., $\Delta\rho = \rho_{D_2O} - \rho_{CTAT} = 6.14 \times 10^{10}$ cm^{-2} in excellent agreement with the fitted contrast (we use for D_2O $\rho_{D_2O} = 6.39 \times 10^{10}$ cm^{-2} .[23]

Although impressive in the high q region, the adjustment to the data using eq 2 stresses the difficulty involved in determining a characteristic length L for the cylindrical objects using SANS data. In neither of the above cases (salted or salt-free) is this derivation straightforward.[24] From the comparison provided in Figure 8, however, one can deduce that the origin of the correlation peak in salt-free solutions is due to electrostatic repulsive interactions between cylindrical species. The location of the maximum scattering at q_{Max} defines a typical distance within the medium, which will be specified in the following. Adding electrolyte not only decreases the range and strength of the electrostatic potential, but also favors the micellar growth. In the 0.2 M NaCl solution, the micelles are extremely long and entangled, as revealed by a static viscosity of 150 times that of the solvent. For comparison, the static viscosity for CTAT/D_2O at 0.41% is only 1.7 mPa s, which in turn is an indication that the micellar aggregates are most likely rodlike.

The upturn of the intensity visible in the spectrum of Figure 8 for the $\phi = 0.41\%$ salted solution at low wave vector is due to the finite persistence length of the micellar chain.[25,26] Recently, Brûlet and co-workers[23,27] have proposed an analytical expression for the form factor of

(23) Cotton, J.-P. In *Diffusion des Neutrons aux Petits-Angles*; Cotton, J.-P., Nallet, F., Eds.; EDP Sciences: Albé, Massif Vosgien, France, 1998; Vol. 9, pp 21−49.

(24) Schneider, J.; Karrer, D.; Dhont, J. K. G.; Klein, R. *J. Chem. Phys.* **1987**, *87*, 3008.

(25) Appell, J.; Bassereau, P.; Marignan, J.; Porte, G. *Prog. Colloid Polym. Sci.* **1990**, *81*, 13−18.

(26) Marignan, J.; Appell, J.; Bassereau, P.; Porte, G.; May, R. P. *J. Phys. Fr.* **1989**, *50*, 3553−3566.

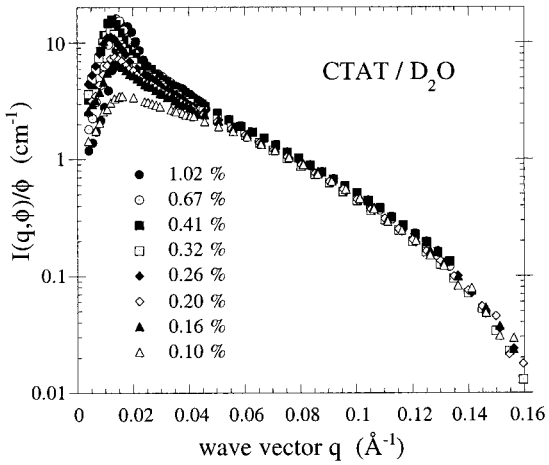

Figure 7. Semilogarithmic plot of the normalized intensity $I(q,\phi)/\phi$ versus q for CTAT concentration ranging from 0.10 to 1.02%. At large wave vectors ($q > 0.05$ Å^{-1}) all sets of data collapse onto the same master curve, whereas strong deviations are observed at lower q.

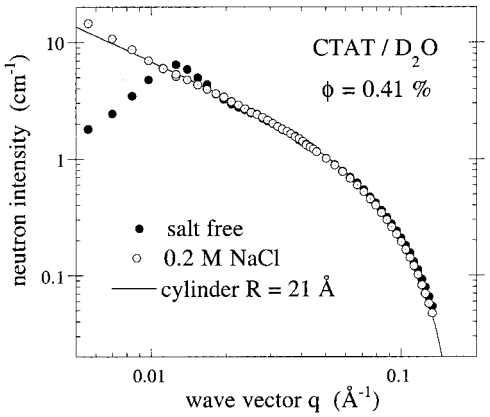

Figure 8. Comparison between the absolute neutron intensities $I(q)$ as received from two CTAT solutions at $\phi = 0.41\%$ and 25 °C. The first is free of added salt (closed circles, the data are those of Figure 6d), whereas the second was prepared with excess of sodium chloride (0.2 M, empty circles). The continuous line is calculated according to eq 2 for an assembly of disordered cylindrical micelles of length L (monodisperse) using $R = 21 \pm 0.4$ Å and $\Delta\rho = 6.12 \times 10^{10}$ cm^{-2}.

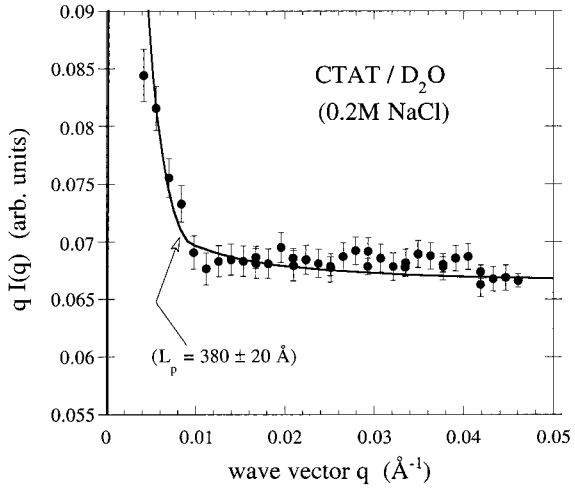

Figure 9. $qI(q)$ versus q in linear scales for the $\phi = 0.41\%$ salted solution, see Figure 8. The result of best fit calculations using an analytical expression for the form factor of semiflexible chains[27] is shown as a continuous line, using for the persistence length of the micellar chains $l_p = 380 \pm 20$ Å.

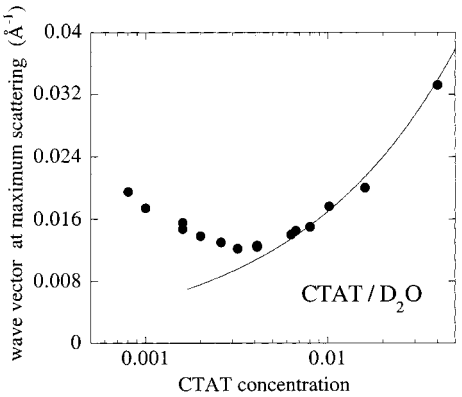

Figure 10. Location of the maximum neutron scattering measured in CTAT/D_2O as function of the concentration ($\phi = 0.08-4\%$). The minimum observed in $q_{Max}(\phi)$ indicates the overlap concentration ($\phi^* = 0.35 \pm 0.05\%$) between the dilute and semidilute regimes. Above ϕ^* the data are represented well by a power law variation with an exponent $^1/_2$. The continuous curve is computed according to eq 3 with $R = 22.5$ Å.

persistent chains. Based on the model of a wormlike chain according to Kratky and Porod and on exact calculations due to des Cloizeaux,[23] this expression exhibits an upturn of the intensity within the $1/q$ regime at a wave vector $\sim 3.2/l_p$, where l_p is the persistence length of the wormlike micelle. In Figure 9, the product $qI(q)$ is plotted versus q using linear scales in order to emphasize this upturn. Calculations using the expression from Brûlet et al. were performed, and the persistence length can be determined quite accurately. The continuous line in Figure 9 corresponds to $l_p = 380$ Å, with an uncertainty of l_p less than 5%. This is a typical value for persistence length in wormlike micelles. In the following subsection, we investigate the $q_{Max}(\phi)$ dependence and characterize the concentration regime in CTAT/D_2O.

IV.2. The Correlation Peak. Figure 10 shows the position of the maximum scattering of CTAT/D_2O from $\phi = 0.08$ to 4%. With increasing ϕ, $q_{Max}(\phi)$ first decreases, passes through a minimum around $\phi^* = 0.35 \pm 0.05\%$, and then increases again. Below $\phi = 0.08\%$, the neutron intensity is weak due to the low number density of scattering particles. The behavior above ϕ^* follows a power law variation, $q_{Max}(\phi) \sim \phi^{1/2}$, that is usually expected for strongly interacting cylindrical assemblies in semidilute regime. More quantitatively, assuming a locally hexagonal arrangement of the cylindrical micelles at the scale of the blob, the concentration ϕ is related to the position in q space of the first maximum of the structure factor

$$q_{Max}(\phi) = \frac{(8\pi)^{1/2}}{3^{1/4}R}\sqrt{\phi} \qquad (3)$$

Equation 3 is plotted as the solid line in Figure 10 using $R = 22.5$ Å as the only input parameter. The agreement with the previous determination of the cylindrical radius of CTAT micelles (according to eq 2) is astonishingly good. Therefore, keeping in mind that eq 3 is observed at concentrations where the solutions are undoubtedly viscoelastic ($\eta_0 \gg \eta_s$ as in Figure 5), we conclude that the regime $\phi > \phi^*$ is semidilute. The characteristic distance of the medium (which is of the order of $1/q_{Max}$, approximately hundreds of angstroms for the CTAT solu-

(27) Brûlet, A.; Boué, F.; Cotton, J.-P. *J. Phys. II Fr.* **1996**, *6*, 885–891.

tions) can be seen as the mesh size of the semidilute regime. In this regime, this length scale is by far much smaller that the average curvilinear length of the micellar objects. Then, one has $1/q_{Max} \ll L$.

In Figure 10, we interpret the deviation of $q_{Max}(\phi)$ with respect to the $\phi^{1/2}$ dependence as the signature of the onset of the dilute regime. Assuming a locally face-centered cubic symmetry, the typical distance $\bar{d}$ between centers-of-masses of rodlike particles will be $\bar{d} = \pi\sqrt{6}/q_{Max}$ and therefore $\bar{d} > L$. The initial decrease of the $q_{Max}(\phi)$ below ϕ^* is an essential result. It means that $\bar{d}$ increases with concentration, a result that can only be understood as an indication of the linear growth of the rodlike aggregates. This reasoning can be formulated in a more quantitative way. Let us call $n(\phi)$ the number density of (monodisperse) rods of lengths $L(\phi)$ and radius R in the dilute regime. The volume fraction conservation law requires the proportionality

$$n(\phi)\, L(\phi)R^2 \sim \phi \tag{4}$$

Since $n(\phi) \sim 1/d^3 = (q_{Max}/\pi\sqrt{6})^3$, the initial decrease of $q_{Max}(\phi)$ as observed in Figure 10 is compatible with a growth of micellar chains, or an increase in $L(\phi)$.

IV.3. A Quantitative Model. In our first report on the CTAT system,[15] we used a quantitative model in order to fit the neutron scattering data, the objective being the determination of an average length L of the rodlike particles in the dilute regime, i.e., $\phi < \phi^*$ (or equivalently $n(\phi)L^3(\phi) \ll 1$, or $L(\phi) \ll \bar{d}$). Basically this model computes the form factor of monodisperse cylinders (length L, radius R) and the structure factor $S(q)$ arising from the electrostatic interactions. For the calculation of $S(q)$, we assume that there are no orientational correlations between neighboring particles, and thus the interaction potential is considered to be simply isotropic. This condition is met as long as the rods are short with respect to the intermicellar distance (dilute regime). This ensures in addition that the rotational diffusion constant $D_r(L)$ is large, which is again a necessary condition to treat the interactions as arising from pointlike objects. The scattered amplitude of homogeneous cylinder of radius R and full length L is[23]

$$F(q) = 2V_c\Delta\rho \frac{J_1(qR \sin\beta)}{qR \sin\beta} \frac{\sin((qL/2)\cos\beta)}{(qL/2)\cos\beta} \tag{5}$$

where $V_c = \pi R^2 L$ is the volume of the cylinder and β is defined as the angle between the vector q and the rod axis. To account for the electrostatic interactions between the charged supramolecular aggregates, the structure factor $S(q)$ is calculated using the Hayter−Penfold procedure,[28] with the renormalization of Hansen and Hayter.[29] The intensity scattered by identical homogeneous objects with only positional correlation is given by[23]

$$I(q) = n(\phi)(|\langle F(q)\rangle|^2 S(q) + \langle |F(q)|^2\rangle - |\langle F(q)\rangle|^2) \tag{6}$$

where the brackets $\langle\ \rangle$ indicate an average over all orientations of the rods. The adjustable parameters entering eqs 5 and 6 are the length L, the scattering contrast $\Delta\rho$, the effective charge Q per aggregate and the Debye length λ_D. The radius was kept ϕ-independent at $R = 20.5$ Å (see Figure 8). As mentioned before, the scattering length density can be calculated for CTAT amphiphiles with respect to the solvent, but since it is a prefactor to the overall intensity, we kept it as a fitting parameter and check a posteriori the concordance with the estimated value ($\Delta\rho = 6.14 \times 10^{10}$ cm^{-2}). The two last quantities, Q and λ_D, are important in defining the shape and the range of the electrostatic potential. They depend actually on the degree of dissociation of the tosylate ions. In agreement with ref 30,[30] we assume that there is around 5−10% of free tosylate counterions in the solution, the remaining being part of the micellar body. Calculations using eqs 5 and 6 are shown as continuous lines in Figure 6a−d for $\phi = 0.10-0.41\%$, and the agreement is acceptable.[15] The values of the adjustable parameters L, Q, λ_D, and $\Delta\rho$ arising from the fits are listed in Table 2, as well as the number density $n(\phi)$ of particles and the corresponding average distance between neighboring cylinders. These findings deserve the following comments:

Table 2. Values of Adjustable Parameters Used in the Model Calculation of SANS Data Obtained on CTAT/D_2O, Shown as Continuous Lines in Figure 6[a]

ϕ (%)	L (Å)	Q (e)	λ_D (Å)	$\Delta\rho$ (10^{10} cm^{-2})	$\bar{d}$ (Å)	n (10^{15} cm^{-3})
0.10	90	10	300	5.7	490	8.5
0.16	155	15	300	6.3	500	8.0
0.26	400	22	200	6.1	590	4.9
0.41	550	41	100	6.9	560	5.6

[a] The adjustable parameters entering the model are the length L, the effective charge Q per aggregate, the Debye length λ_D, and the scattering contrast $\Delta\rho$. The difference of scattering length densities determined from fits should be compared to the one estimated for the CTAT molecule in D_2O ($\Delta\rho = 6.14 \times 10^{10}$ cm^{-2}). The intermicellar distance $\bar{d}$ is provided by the fits, and the number density of particles n is calculated from the $\bar{d}$ values. The radius of the cylindrical self-assemblies was kept ϕ-independent at $R = 20.5$ Å.

(i) Once the concentration is fixed, the position of the maximum in the scattering curve is extremely sensitive to the length of the rods. The $L(\phi)$ data displayed in Table 2 are found within an error less than 5%.

(ii) The total charge on the aggregates determines the width of the scattering peak, while the Debye length plays a minor role in the fitting procedure. From the data in Table 2, we deduce that the cylinders are carrying one effective charge every 10−20 Å along its length, according to the concentration. This result is in agreement with a 5−10% dissociation of the tosylate counterions.

(iii) Finally, except for $\phi = 0.41\%$, we found $\Delta\rho$ values in relative agreement with that calculated for CTAT in D_2O (i.e., within 8%).

As a result, and in agreement with the ϕ dependence of the correlation peak analyzed in the previous subsection, we confirm with this more quantitative model that for CTAT/D_2O the dilute regime extends up to $\phi^* = 0.35\%$. For $\phi = 0.41\%$, the necessary condition imposed initially is not fulfilled, since the intermicellar distance is found of the order of the rod length (Table 2). The variation of the length of the rodlike particles versus concentration is shown in Figure 11. In the dilute regime, $\phi < \phi^*$ where the model applies, the scaling law is found, $L(\phi) \sim \phi^{3/2}$. The results of the quantitative electrostatic model are compared to a direct estimation using eq 4, which includes the volume conservation law. In eq 4, the particle density is assumed to scale with the wave vector at maximum scattering as $n(\phi) \sim (q_{Max})^3$. This second estimate yields a power law with an exponent ~ 2. This comparison demonstrates that even though the kind of relationships such as eq 4 are very rough, as a first approximation, they are probably sufficient to predict the qualitative behavior

(28) Hayter, J. B.; Penfold, J. *Mol. Phys.* **1981**, *42*, 109−118.
(29) Hansen, J. P.; Hayter, J. B. *Mol. Phys.* **1982**, *46*, 651−656.
(30) Narayanan, J.; Mendes, E.; Manohar, C. *J. Phys. Chem.* **1996**, *100*, 18524−18529.

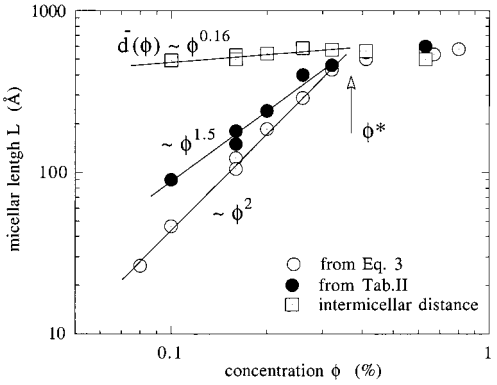

Figure 11. Variation of the average length of the rodlike particles versus concentration, as determined from the quantitative electrostatic model (closed circles, section IV.3). In the dilute regime a scaling is found, $L(\phi) \sim \phi^{3/2}$. Also plotted here are the results of the micellar lengths estimated from the position of the maximum scattering intensity at $q_{Max}(\phi)$ (eq 4) and the mean intermicellar distance $\bar{d}$.

of the strongly interacting micellar objects. Deviations between both derivations are evidenced below $\phi = 0.10\%$. Finally, the intermicellar distance $\bar{d}$ derived from the model (see column 6 in Table 2) is also plotted in Figure 11. As mentioned before, both $L(\phi)$ and $\bar{d}(\phi)$ variations cross at $\phi = \phi^* = 0.35\%$, further justifying our claim that ϕ^* is 0.35% for CTAT in D_2O.

Concerning the electrostatic model used to adjust the neutron scattering data (dilute regime), we are aware of some of its weaknesses. In applying the model, we have assumed that the scattering particles were monodisperse in length. This is a restrictive conjecture that was only justified by the fact that reasonably good fits (those of Figure 6) could be obtained with the simplest model. We are also aware that polydispersity effects would shift the first oscillation of the structure factor to lower wave vector.

V. Discussion

In this section the emphasis will be on the comparison between the previous results and the literature data on CTAT, as well as the predictions of a model by MacKintosh[31] on the growth of electrostatically interacting micellar rods.

V.1. Comparison with CTAT Literature Data. The amphiphilic salt of cetyltrimethylammonium tosylate has been investigated for a decade or so, and a wealth of information is available in the recent literature. CTAT in dilute solution was studied by electric birefringence,[30] by FRAPP,[32,33] and by cryo-TEM.[34] At higher concentrations, $\phi > 4\%$ extensive rheological measurements were undertaken and reported by Soltero and co-workers.[35−37] As far as the dilute solutions are concerned, the conclusions of the analysis provided in the former section are in good qualitative agreement with the works by Narayanan and co-workers. At low concentration in H_2O, the dilute regime is found to extend up to $\phi^* = 0.7\%$,[32,33] a result that does not contradict the static viscosity measurements of Figure 5 (see also Table 1 for comparison). Note that the change from H_2O to D_2O slightly shifts the overlap concentration to lower ϕ, the physics remaining the same. The lengths of the rodlike particles as determined from electric birefringence (several hundreds of angströms) have the correct order of magnitude in the low ϕ regime. For instance, in CTAT/H_2O Naranayan et al. derived a length of 370 Å at $\phi = 0.2\%$[30] and an effective charge by unit length of 0.14 e/Å.[33]

However, in contradiction to the electric birefringence data,[30] we do not find any evidence of the scaling law $L(\phi) \sim \phi^{0.5}$ that was predicted for neutral micelles. Estimation of the electrostatic potential between the CTAT rods in the dilute regime, and in agreement with the structure factor seen in neutron scattering, enables us to conclude that the micellar objects experience strong repulsive interactions and that, if any theory should apply, the one by MacKintosh et al. might be the appropriate one.[31] The second disagreement with previous reports on CTAT is a freeze−fracture electron replica reported by Kaler et al.[34] This replica of a solution of 0.1% CTAT in water shows a huge micelle of several microns, rather rigid and with a average diameter of 50 Å. If such large macromolecules are present in the equilibrated solutions of CTAT submitted to the neutron flux, there is little chance that this technique could detect it. On the other hand, one has to be sure that, in the preparation procedure of the replica of ref 34, the sample has not been sheared. In this respect 1−5 demonstrated that the rheological properties of dilute CTAT solutions are rather unusual, and new (micro)-structures might be induced by simple shearing.

V.2. Comparison with MacKintosh's Model.[31] The only model (to our knowledge) that describes the growth dynamics of charged rodlike micelles was due to MacKintosh, Safran, and Pincus.[31] In this model, the end-cap energy is assumed to be balanced by the electrostatic interactions between surface charges belonging to the same linear aggregate. However, the MacKintosh model does ignore the electrostatic repulsion between charged aggregates. As a result, the rod length is found to be nearly constant in the dilute regime, and then above ϕ^*, $L(\phi)$ is characterized by a more rapid growth than for neutral micelles. For neutral micelles, we recall that the scaling law $L(\phi) \sim \phi^{1/2}$ was predicted.[38,39] Obviously the present SANS data on CTAT are not agreeing with the MacKintosh predictions. Rather, scaling exponents around 1.5−2 have been found for $L(\phi)$ in Figure 11, below the overlap concentration. One possible reason for this disagreement could be that the concentration range investigated by SANS ($\phi > 0.08\%$) is already too high for the MacKintosh model to apply. The existence of a structure factor different from unity clearly attests to the role played by the intermicellar interactions. The range of validity of the MacKintosh model for CTAT is therefore restricted to still lower ϕ (down to the second critical micellar concentration, 0.04%[35]).

V.3. Shear-Thickening Transition. In our first paper on CTAT dilute solutions,[15] it was emphasized that the shear-thickening transition was neither a mechanical transition nor a flow instability. With mechanical transition we meant a phenomenon that would have its origin in the mechanical coupling of an anisotropic macromolecule to a shear flow. In this respect, and with referencing to shear-thickening systems, flow-induced gelation was

(31) MacKintosh, F. C.; Safran, S. A.; Pincus, P. A. *Europhys. Lett.* **1990**, *12*, 697−702.
(32) Narayanan, J.; Manohar, C.; Langevin, D.; Urbach, W. *Langmuir* **1997**, *13*, 398−401.
(33) Narayanan, J.; Urbach, W.; Langevin, D.; Manohar, C.; Zana, R. *Phys. Rev. Lett.* **1998**, *81*, 228−231.
(34) Kaler, E. W.; Herrington, K. L.; Murthy, A. K.; Zasadzinski, J. A. N. *J. Phys. Chem.* **1992**, *96*, 6698−6707.
(35) Soltero, J. F. A.; Puig, J. E.; Manero, O.; Schultz, P. C. *Langmuir* **1995**, *11*, 3337−3346.
(36) Soltero, J. F. A.; Puig, J. E.; Manero, O. *Langmuir* **1996**, *12*, 2654−2662.
(37) Soltero, J. F. A.; Bautista, F.; Puig, J. E.; Manero, O. *Langmuir* **1999**, *15*, 1604−1612.
(38) Cates, M. E. *Macromolecules* **1987**, *20*, 2289−2296.
(39) Cates, M. E. *J. Phys. Fr.* **1988**, *49*, 1593−1600.

predicted.[11,40] The basic reasoning of shear-induced gelation takes into account the kinetic equations for scission and fusion of neighboring micelles. The competition between the rotational Brownian diffusion of rods and the effect of the convective flow field is also considered. The shear-induced gelation is obtained when neighboring rods fuse together if the flow forces them to be collinear. It is then suggested that a "network" (gel) of extremely large aggregates is formed. Critical velocity gradients can be estimated by comparing the applied shear rate at the transition and the rotational diffusion constant $D_r(L)$ of rods of length L. Simple scaling yields[40]

$$\dot{\gamma}_c \sim D_r(L) \sim k_B T/\eta_s L^3 \quad (7)$$

where η_s is the viscosity of the suspending solvent. Equation 7 emphasizes that the longer the rodlike particles, the easier they are aligned and, thus, the sooner is the transition. Underlying eq 7, there is the expectation that with increasing concentration, $\dot{\gamma}_c$ should decrease. In the literature there are several surfactant systems that exhibit the previous behavior, namely a decrease of $\dot{\gamma}_c$ versus concentration, e.g., Gemini 12-2-12,[8,9] or CTAB/NaSal systems.[21] Nevertheless, in view of the present experimental findings on CTAT, eq 7 is inconsistent with our results at least on two aspects. First, for average micellar lengths around 100−500 Å as shown in Figure 11, the diffusion rotational constant D_r is as high as 10^5−10^6 s^{-1}. These orders of magnitude do not compare with the critical shear rates of 10 s^{-1} that are actually measured. Second, if eq 7 were to be valid, huge variations of the critical rate $\dot{\gamma}_c$ would be expected upon varying ϕ. For CTAT/D_2O, the transition is observed over a quite broad concentration range including both dilute and semidilute regimes. Over more than one decade in ϕ, the critical rate is found to weakly increase with concentration, at best by a factor 5 (see Figure 5).

VI. Concluding Remarks

In this paper, we have studied the nonlinear steady shear properties of dilute solutions of CTAT surfactant, in the concentration range $\phi < 1\%$. First, we outlined the features of the shear-thickening transition, which is a transition between two different rheological states of the same dilute surfactant solution. One is a Newtonian and fluid at low shear rates, the second is more viscous, induced by shear and observed only above a characteristic shear rate $\dot{\gamma}_c$. The evolution of the critical rate as function of the amphiphile concentration and temperature is determined experimentally: $\dot{\gamma}_c$ varies strongly with T, according to an Arrhenius behavior, but very weakly with concentration. In contradiction with recent reports on a different surfactant system,[12] the transition toward the shear-induced viscous state and under strain-controlled conditions is continuous in the CTAT/H_2O systems.

Neutron scattering experiments have been performed at rest on a broad concentration range to correlate the shear properties to the equilibrium micellar structure. The more salient conclusions are (i) for all concentrations investigated ($\phi = 0.08$−0.8%, solvent D_2O) that display the thickening transition, the local morphology is that of cylindrical micelles, with a radius $R = 21.0 \pm 0.5$ Å; (ii) all spectra exhibit a scattering correlation peak due to the electrostatic interactions between charged micelles; and (iii) the zero-shear rheology and SANS data recorded at rest agree with characteristic concentration regimes.

One fundamental conclusion of this study is that the shear-thickening transition has the same features and thus, according to us the same physical origin for solutions prepared in the dilute ($\phi < \phi^*$) and in the semidilute ($\phi^* < \phi < 0.8\%$) regimes where $\phi^* = 0.35\%$ is the overlap concentration in CTAT/D_2O. Still more astonishing, the thickening occurs at (almost) the same shear rate along this dilution line, being thus independent of the concentration.

Our rheological and neutron data clearly demonstrate that the shear-thickening transition takes place in the dilute regime, that is, the regime where the aggregates are short and unentangled rods (say below $\phi = 0.1\%$). Even if the microscopic mechanisms are not elucidated here, it is likely that the shearing induces the growth of the cylindrical micelles. In passing, note that thermodynamic and physicochemical variables such as the salt content (Figure 8), the temperature, and the concentration itself (Figure 5) are able to promote the growth of the micellar aggregates. Therefore, the shear-thickening transition is a transition between two states corresponding to two very different self-assembling properties. At rest and in regime I, a dilute solution ($\phi < \phi^*$) is a dispersed system where the majority of the aggregates are short rodlike and unentangled particles. In our notation, this corresponds to an average length L much shorter than the intermicellar distance $\bar{d}$. On the other hand, the thickened state is the extrapolation at high shear rates of a viscoelastic solution of entangled wormlike micelles. If this state could exist at rest, it would be characterized by micellar lengths much longer than the mesh size of the network. The present study finally suggests that electrostatics play a crucial role.

Acknowledgment. R.G.-C. and J.-F.B. thank the Laboratoire Léon Brillouin (CEA Saclay, F-91191 Gif/Yvette, France) for its experimental and financial support during the course of the neutron experiments. We also acknowledge GDR 1081 "Rhéophysique des Colloides et Suspensions" of the CNRS for a stimulating environment. The present work is partly funded by the European Community (Contract No. FMRX-CT96-0003).

LA990187B

(40) Bruinsma, R.; Gelbart, W. M.; Ben-Shaul, A. *J. Chem. Phys.* **1992**, *96*, 7710−7727.